Microwave Imaging Based on Time Reversal Mirror for Multiple Targets Detection

Tong Mu and Yaoliang Song

School of Electronic and Optical Engineering
Nanjing University of Science and Technology, Nanjing, 210094, China
mutong@njust.edu.cn, ylsong@njust.edu.cn

Abstract ─ Time reversal (TR) is an applicable technique for target detecting and has gained extensive attention due to its self-adaptive focusing ability. However, the imaging performance of the traditional time reversal mirror (TRM) deteriorates in multiple targets cases. A TR imaging approach for multiple targets detection is proposed in this paper. Different from the direct retransmission of the TR signals, the time domain gating is applied to the targets responses to divide them into different groups, and the optimal time frame corresponding to each target which will be utilized in the subsequent step is calculated. After the retransmission of the gated TR signals, the essential zero setting step and the summation step are conducted to construct the imaging function. Numerical simulations are carried out for three multi-targets cases using the finite-different time-domain (FDTD) method. The imaging results are compared with the traditional TRM method and indicate the effectiveness and the superiority of the proposed approach.

Index Terms ─ Multi-targets detecting, optimal time frame, time domain gating, time reversal.

I. INTRODUCTION

Time reversal (TR) technique was first proposed in acoustics [1] and then introduced to electromagnetics [2]. It exploits the invariance of the wave equation in lossless and time-invariant media, and involves physical or synthetic retransmission of signals received by a TR array (TRA) in a time reversed fashion. Time reversal has found applications in various disciplinary fields such as microwave imaging [3,4], wireless communication [5,6] and nondestructive testing [7,8], etc.

Time reversal mirror (TRM) is the direct implementation of time reversal and performs as an effective technique for the detection and localization of targets. Traditional TRM method contains two main steps. In the first step, the probing signal is emitted from the transmitter and the signals scattered from the targets are recorded by the TRA. In the second step, the recorded signals are time reversed and retransmitted by the corresponding receiver in TRA. Then the back-propagated signals will focus around the target positions, and the total field values in the imaging domain at the focusing instant are used for imaging the targets. Although the traditional TRM is easy to accomplish, its performance deteriorates in multiple targets cases. Specifically, images of targets especially the further and weaker ones may be disturbed or swamped by the nearer and stronger ones, and false results will be obtained if the targets are located closely to each other. The iterative TRM method [9] conducts the signal reception, reversal and retransmission iteratively and achieves focusing on the strongest target, but it is still unable to detect the weaker targets. The TR imaging method proposed in [10] uses the grouping technique that divides the TRA into different sub-TRAs and discriminates multiple targets by enhancing the synchronism at target positions. However, the signals need to be retransmitted many times as the number of sub-TRAs should be large enough to ensure the coherence at target positions and the incoherence at non-target positions, which makes it time-consuming to some degree.

The imaging techniques based on the TR operator (TRO) have raised concern in recent years. They include the decomposition of the TR operator (DORT) and the TR multiple signal classification (TR-MUSIC). Selective imaging for different targets can be achieved by the DORT [11,12], and simultaneous multi-targets imaging can be achieved by the TR-MUSIC [13,14]. For the acquisition of the TRO, both the two methods require a large number of measurements to construct the multistatic data matrix (MDM). Specifically, each transceiver transmits signal to the detecting region in sequence, and the scattered signals are recorded by all transceivers after each transmission, causing heavy computation and making it time-consuming for data collection. In addition, the number of targets should not exceed the number of transceivers, limiting the practical applications of these methods.

In this paper, a new TR imaging scheme based on the TRM is proposed for multiple targets detection. First, the signals scattered from the targets are recorded by TRA, and the time domain gating technique is applied at

Submitted On: June 22, 2017
Accepted On: October 19, 2018

each receiver to divide the signals into different groups corresponding to different targets. The time domain gating is able to eliminate unwanted responses from other targets by using a gating filter, and it is also effective for noise reduction [15]. After that the target initial reflection method (TIRM) [16] is used to obtain the focusing instant for each target. Next, the gated signals are time reversed and retransmitted in sequence and the field values in the imaging domain at each time frame are recorded correspondingly. Then, the zero setting is conducted and the recorded field values are added up to construct the imaging function. The images of different targets can be obtained by selecting different time frames, and simultaneous multi-targets imaging can be achieved by applying the normalization and summation steps. Numerical simulations are carried out for three multi-targets cases and the results are compared with the traditional TRM method. It turned out that the proposed approach is simple for implementation and it is able to detect multiple targets synchronously with only one transmitter. It overcomes the near-far problem and the focusing false in multi-targets cases, and also, is more efficient than the TRO based methods.

II. TR IMAGING SCHEME

A. TRM method

Let us consider the 2-D scene with a TRA consisting of N antennas. A probing pulse $x(t)$ is emitted from the transmitter located at $\mathbf{r}_t$ and the signals scattered from the point-like targets are recorded by TRA. The target with the scattering potential ρ_s is located at $\mathbf{r}_s$ and the nth antenna is located at $\mathbf{r}_n$. The incident signal at the target position $\mathbf{r}_s$ in the frequency domain is given by:

$$X_{\text{in}}(\omega) = G(\mathbf{r}_t, \mathbf{r}_s, \omega) X(\omega), \tag{1}$$

where $X(\omega)$ is the Fourier transform of $x(t)$, and $G(\mathbf{r}_t, \mathbf{r}_s, \omega)$ is the Green's function from the transmitter location $\mathbf{r}_t$ to the target position $\mathbf{r}_s$ which represents the "propagator". For notational simplicity the scalar field and Green's function are considered in the theoretical analysis. Extension to the vector case is straightforward in principle but complicated for expression in general form.

The received signal at the nth receiver can be represented as:

$$X_{\text{r}}(\mathbf{r}_n, \omega) = G(\mathbf{r}_s, \mathbf{r}_n, \omega) G(\mathbf{r}_t, \mathbf{r}_s, \omega) X(\omega) \rho_s. \tag{2}$$

If we take the complex conjugate of $X_{\text{r}}(\mathbf{r}_n, \omega)$ which is equivalent to the time reversal in the time domain and then back-propagate it from the nth antenna, we can obtain the total signal at the observation point $\mathbf{r}$ in the imaging domain:

$$X_{\text{TR}}(\mathbf{r}, \omega) = \sum_{n=1}^{N} G(\mathbf{r}_n, \mathbf{r}, \omega) X_{\text{r}}^{*}(\mathbf{r}_n, \omega), \tag{3}$$

where "$*$" denotes the complex conjugate.

Substituting (2) into (3) yields:

$$\begin{aligned} X_{\text{TR}}(\mathbf{r}, \omega) = \sum_{n=1}^{N} & G(\mathbf{r}_n, \mathbf{r}, \omega) G^{*}(\mathbf{r}_s, \mathbf{r}_n, \omega) \\ & G^{*}(\mathbf{r}_t, \mathbf{r}_s, \omega) X^{*}(\omega) \rho_s. \end{aligned} \tag{4}$$

According to the spatial reciprocity principle, we have:

$$G(\mathbf{r}_s, \mathbf{r}_n, \omega) = G(\mathbf{r}_n, \mathbf{r}_s, \omega), \tag{5}$$

and when the observation point $\mathbf{r}$ happens to be the target positon $\mathbf{r}_s$, (4) can be rewritten as:

$$\begin{aligned} X_{\text{TR}}(\mathbf{r}_s, \omega) = \sum_{n=1}^{N} & G(\mathbf{r}_s, \mathbf{r}_n, \omega) G^{*}(\mathbf{r}_s, \mathbf{r}_n, \omega) \\ & G^{*}(\mathbf{r}_t, \mathbf{r}_s, \omega) X^{*}(\omega) \rho_s. \end{aligned} \tag{6}$$

The corresponding time domain representation of (6) can be described as:

$$\begin{aligned} x_{\text{TR}}(\mathbf{r}_s, t) &= \frac{1}{2\pi} \int [\sum_{n=1}^{N} G(\mathbf{r}_s, \mathbf{r}_n, \omega) G^{*}(\mathbf{r}_s, \mathbf{r}_n, \omega) \\ &\quad G^{*}(\mathbf{r}_t, \mathbf{r}_s, \omega) X^{*}(\omega) \rho_s] e^{j\omega t} d\omega \\ &= \sum_{n=1}^{N} G(\mathbf{r}_s, \mathbf{r}_n, t) \otimes G(\mathbf{r}_s, \mathbf{r}_n, -t) \\ &\quad \otimes G(\mathbf{r}_t, \mathbf{r}_s, -t) \otimes x(-t) \rho_s, \end{aligned} \tag{7}$$

where "$\otimes$" denotes the time domain convolution.

Here $G(\mathbf{r}_s, \mathbf{r}_n, t) \otimes G(\mathbf{r}_s, \mathbf{r}_n, -t)$ represents a matched filter which achieves the maximum output at $t = 0$. The signals back-propagated from N antennas will synchronously achieve their maximum values at the target position $\mathbf{r}_s$ at the same instant which is called the optimal time frame. As a result, the field value at the target position is much larger than that of non-target locations thus the target image can be acquired at the optimal time frame by scanning the field value for each point in the imaging domain.

B. Partition of echo signals

According to the analysis above, the target can be detected precisely by the traditional TRM method when there is only one target. If the target positon changes, the optimal time frame changes as well due to the space-time matching property of TR. Now we assume that there are two point-like targets located at $\mathbf{r}_1$ and $\mathbf{r}_2$ respectively. The signals recorded by TRA are the sum of the signals scattered from the two targets and contain the spatial information of both them. If the signals are time reversed and back-propagated directly, the signal components corresponding to the first target will achieve their maximum values synchronously at $\mathbf{r}_1$ at an instant t_1, and the signal components corresponding to the second one will achieve their maximum values synchronously at $\mathbf{r}_2$ at t_2, generally $t_1 \neq t_2$. The intensity of the total field focusing at the first target is also different from that of

the second one.

As a result, if we choose one of the two instants as the optimal time frame, we can only obtain the image of one target which may be disturbed and swamped by the field focusing somewhere else in the imaging domain especially when this target is the weaker or the further one. The deterioration increases as the number of targets grows. To solve this problem, we introduce a new TR imaging scheme, the core idea of which is the partition of the responses from different targets. For this purpose, we apply the time domain gating method that selects a region of interest in the time domain and eliminates unwanted responses by adopting the window function.

It is assumed that there are *K* point-like targets and the multi-path reflections are negligibly small, thus the signal received by each antenna is comprised of *K* responses. As is shown in Fig. 1, if the propagation delay of the signal from the *k*th target is t_k, by using a window function from $t_k-\tau$ to $t_k+\tau$ we can extract the response at t_k as well as the target located between $c(t_k-\tau)/2$ and $c(t_k+\tau)/2$. The principle of choosing the window function is appropriately eliminating unwanted responses without damaging the mainlobe of the desired response. Besides, the use of time domain gating also shows effectiveness in noise suppression.

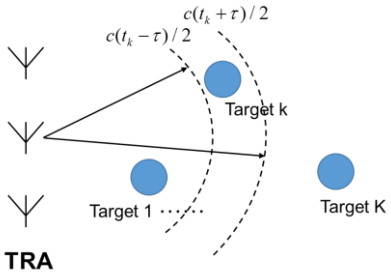

Fig. 1. Illustration of the time domain gating technique.

C. Multiple targets imaging

By applying the time domain gating to all the N received signals, the responses from the *K* targets are divided into *K* groups which can be expressed as

$$\mathbf{Y}=[\mathbf{y}_1,\mathbf{y}_2,...,\mathbf{y}_K], \tag{8}$$

where $\mathbf{y}_k=[\mathbf{s}_{k,1}(t),\mathbf{s}_{k,2}(t),...,\mathbf{s}_{k,N}(t)]^T$, $k=1,2,...,K$ is the *k*th target responses recorded by N receivers, and "T" denotes the transposition. $\mathbf{s}_{k,n}(t)$ with $n=1,2,...,N$ is the 1×*M* signal sequence where *M* is the number of the sampling points in the time domain.

Next, the TIRM algorithm is used to calculate the optimal time frame for each target. The algorithm requires only a few signal parameters and prevails over the traditional methods such as the maximum E-field method and the entropy-based methods. According to the derivation in [16], the optimal time frame is given by:

$$t^{\text{opt}}=\text{maxtime}-\frac{t_r+t_d}{2}, \tag{9}$$

where maxtime is the total duration of the signal propagation, t_r is the instant when the initial reflection from the target arrives at the transmitter antenna, and t_d is the instant when the probing signal reaches its peak value after being excited.

We assume that the transmitter antenna is the n_0th element in the TRA, the instant corresponding to the maximum value of the *k*th target response received by the transmitter antenna is $t_k^{\max}$, and the pulse width of the probing signal is t_p. Therefore (9) can be modified as:

$$t_k^{\text{opt}}=\text{maxtime}-\frac{t_k^{\max}-t_p+t_d}{2}. \tag{10}$$

After the calculation of all the *K* optimal time frames, the *K* groups of signals $\mathbf{y}_1,\mathbf{y}_2,...,\mathbf{y}_K$ are time reversed and retransmitted into the imaging domain in sequence. Thus the field value at each point in the imaging domain is given by:

$$\mathbf{u}_k(\mathbf{r},t)=\sum_{n=1}^{N}\mathbf{s}_{k,n}^{\text{TR}}(\mathbf{r},t)\quad k=1,2,...,K. \tag{11}$$

Now we introduce the essential step: at the optimal time frame we set the elements of $\mathbf{u}_k(\mathbf{r},t)$ corresponding to all the other targets to zero. This step is described as:

$$\mathbf{u}_k(\mathbf{r},t_{k'}^{\text{opt}})|_{k'\neq k}=0\quad k'=1,2,...,K. \tag{12}$$

The zero setting ensures that when the TR signals achieve the maximum value at t_k^{opt} the image of the *k*th target will not be disturbed or swamped by other targets, and it is applicable for both strong and weak targets. Then all the modified $\mathbf{u}_k(\mathbf{r},t)$ are added up to construct the imaging function:

$$\mathbf{U}(\mathbf{r},t)=\sum_{k=1}^{K}\mathbf{u}_k(\mathbf{r},t). \tag{13}$$

Imaging for the *k*th target can be realized by selecting $t=t_k^{\text{opt}}$, and simultaneous multi-targets imaging is given by:

$$\mathbf{F}(\mathbf{r})=\sum_{k=1}^{K}\frac{\mathbf{U}(\mathbf{r},t_k^{\text{opt}})}{U(\mathbf{r}_k,t_k^{\text{opt}})}, \tag{14}$$

where $\mathbf{r}_k$ is the *k*th target position and $U(\mathbf{r}_k,t_k^{\text{opt}})$ is the maximum value of the field intensity recorded in the imaging domain at the focusing instant. The normalization process makes the signals synchronically achieve the value of 1 at each target position. Based on the proposed scheme, the image of each target can be acquired without interference and the images of *K* targets show equal visibility.

The block diagram of the proposed TR imaging approach is depicted in Fig. 2.

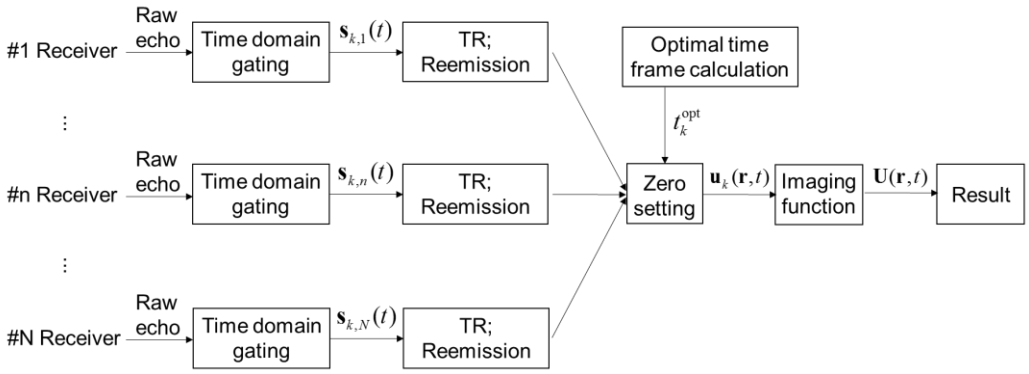

Fig. 2. Block diagram of the proposed approach.

III. SIMULATIONS AND RESULTS

A. Simulation setup

For solving the electromagnetic scattering problem and collecting the waveform data, the TMz polarized 2-D finite-different time-domain (FDTD) method is used in this work. FDTD is a numerical technique that is based on the finite difference approximation of the differential Maxwell's equations [17]. It discretizes the time and space variables in the computational domain by using the Yee cells, and it makes the electric (magnetic) field at each grid point only dependent on the magnetic (electric) field at the adjacent grid point as well as the corresponding component at the last time step. Given the initial value, the future values of the electric and magnetic fields are updated from the previous values at each grid point, thus the spatial distribution of the electromagnetic field can be acquired. The FDTD method calculates the field propagation in the time domain directly and is able to model different objects of study in different coordinates with low computational costs. Therefore, it is appropriate for the numerical solution of forward propagation of the probing signal/target response and back-propagation of the TR signals.

Figure 3 illustrates the setup of the numerical simulation. The imaging domain contains 200×200 FDTD grids and the grid size is set as $\Delta x = \Delta y = 1\,\text{cm}$. The time step is $\Delta t = 16.7\,\text{ps}$ and the maximum iteration time is $\text{maxtime} = 1000\Delta t$. The perfectly matched layers (PML) are applied as the absorbing boundaries to truncate the computational domain and avoid wave reflections on the boundary. Point-like scatterers with radius $r = 3\,\text{cm}$ are located in the detecting region which is considered as the homogeneous medium (free space) in the experiment. The conductivity and the relative permittivity of the scatterers are $\sigma = 0.1\,\text{S/m}$ and $\varepsilon_r = 30$ respectively. It is worth mentioning that in the case of dispersive or lossy medium such as detecting tumor in the breast tissue or sensing target through the brick wall, dispersion or attenuation of the fields caused by the background medium should be taken into account. Also, the corresponding FDTD iterative formulas should be modified depending on the specific case in the modeling, which is out of the scope of this paper. The TRA composed of 10 antennas is equally spaced and located parallel to the Y axis. The interval between adjacent antennas is half of the wave length corresponding to the center frequency of the probing signal. The sinusoidal modulated Gaussian pulse with the center frequency being 2 GHz and the bandwidth being 4 GHz is transmitted by the 5th antenna of the TRA, and the corresponding waveform and frequency spectrum are shown in Fig. 4. The signals scattered from the targets are recorded by the TRA and the Gaussian white noise with the signal-to-noise ratio (SNR) being 25 dB is added to the received signal.

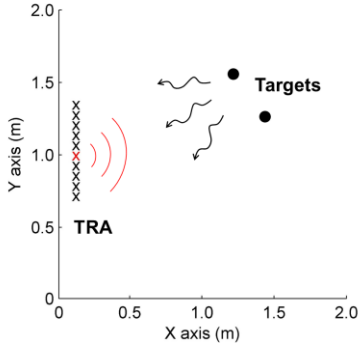

Fig. 3. Setup of the numerical simulation.

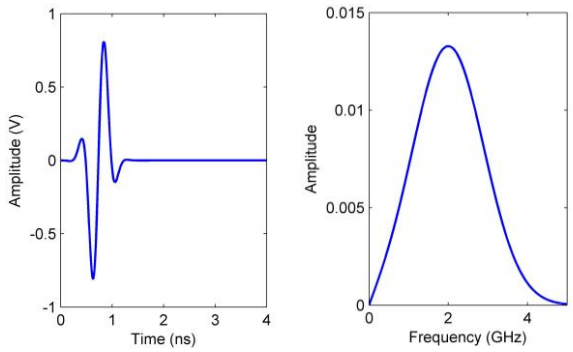

(a) (b)

Fig. 4. Probing signal: (a) time domain waveform and (b) frequency spectrum.

B. Simulation results

Three different multi-targets cases are studied to evaluate the performance of the proposed imaging approach. The numerical results obtained by the proposed method and the traditional TRM method are both provided for comparisons. The TRA is marked with "x" and the actual targets locations are marked with "o" in the resulted images.

In the first case, imaging for two targets located at (0.6 m, 0.8 m) and (1.4 m, 0.8 m) respectively is investigated. After the reception and storage of the echo data, the time domain gating is applied to all the raw signals. The Hanning window is selected as the window function for the numerical experiment. The *k*th time-window for the *k*th target response is given by:

$$f_k(t) = 0.5(1-\cos(\frac{2\pi(t-\delta_k)}{W})), \qquad (15)$$

where δ_k is the time shift and W is the window width. As is analyzed in the second section of the paper, the time shift value is set equal to the propagation delay of the *k*th target response. The window width is chosen depending on the specific circumstance, and it is set as $W = 100\Delta t$ for the numerical experiment.

The raw signal received by the 1st antenna and two corresponding window functions used for target response extraction are shown in Fig. 5. The amplitude values of the actual echo signals are far less than 1, thus the amplitude normalization is applied to the signal to make it visually comparable with the window functions.

Figure 6 shows the imaging results for the targets based on the traditional TRM method. It can be seen that the image of the first target (the nearer one) is accurately obtained while the image of the second target (the further one) is not as bright as the first one, and some interferences can be observed in the image domain. The reason is that the echo from the further target arrives at the TRA later, thus it is emitted from the TRA earlier after being time reversed. When it achieves the maximum value at the further target position, the TR signal for the nearer target is to be emitted or just emitted from the TRA. So if the snapshot is taken at the optimal time frame for the further target, strong fields will appear around the TRA and cause inevitable interferences.

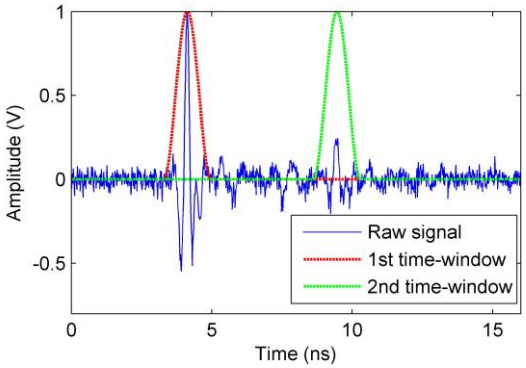

Fig. 5. Raw signal received by the 1st antenna and window functions.

Figure 7 shows the imaging results given by the proposed approach. It can be observed that both of the targets are imaged accurately and clearly without any interference. Besides, the two targets can be imaged synchronously with the same brightness by the normalization process described in (14), as shown in Fig. 7 (c).

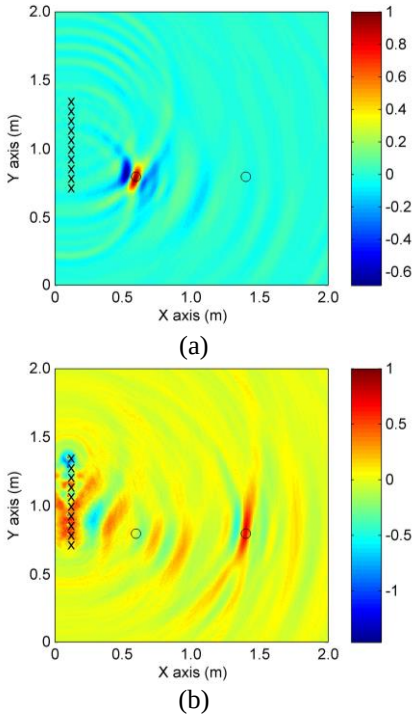

(a)

(b)

Fig. 6. Imaging results for the targets located at: (a) (0.6 m, 0.8 m) and (b) (1.4 m, 0.8 m) by the traditional TRM method.

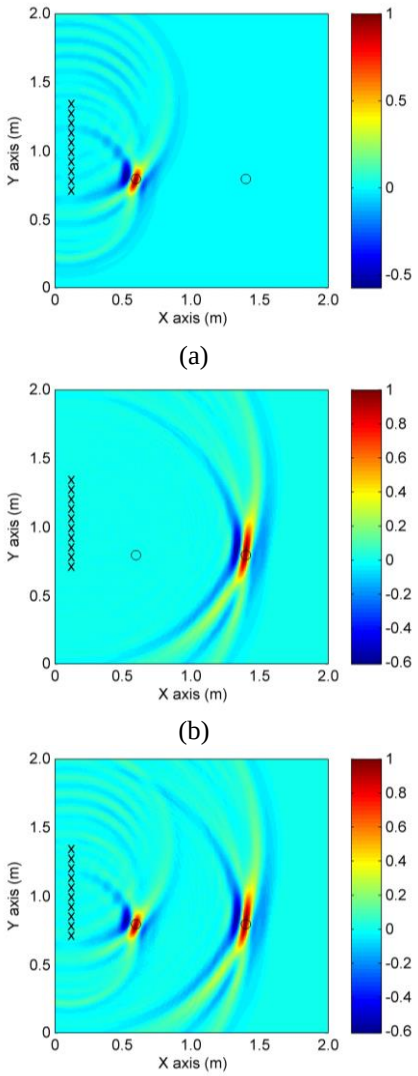

Fig. 7. Imaging results for the targets located at: (a) (0.6 m, 0.8 m), (b) (1.4 m, 0.8 m, and (c) multiple targets by the proposed TR method.

Figure 8 and Fig. 9 show the imaging results for two targets located at (0.6 m, 0.8 m) and (0.75 m, 0.9 m) given by the two methods respectively, representing the case where the targets are located closely to each other. On the one hand, from Fig. 8 (a) we can see that the nearer target is imaged precisely but a darker "ghost image" appears around the further target. It is because that when the back-propagated signals focus at the nearer target, the focusing fields at the further one just diverged. Similarly in Fig. 8 (b), the fields are about to reach the maximum values at the nearer target at the optimal time frame corresponding to the further one, causing a "ghost image" which is even brighter than the image of the further target. Therefore the traditional TRM method fails to detect the further target in this case.

On the other hand, it is shown in Figs. 9 (a), (b) and (c) that the two closely located targets can be both detected successfully and no "ghost image" appears, indicating the effectiveness of the proposed method for the closely-located-targets-case.

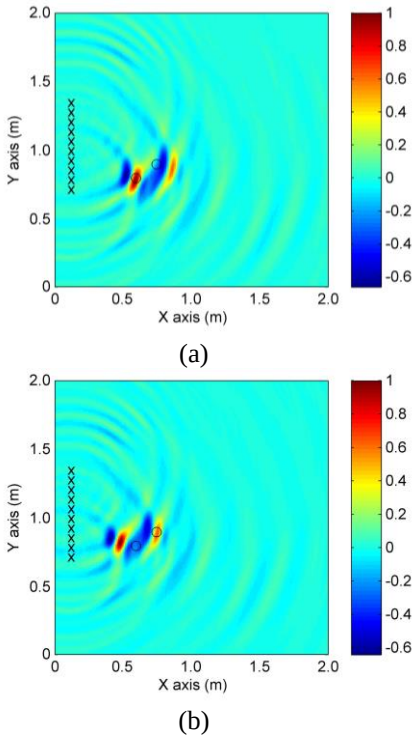

Fig. 8. Imaging results for the targets located at: (a) (0.6 m, 0.8 m) and (b) (0.75 m, 0.9 m) by the traditional TRM method.

In the third case we investigate the detection of three targets located at (0.6 m, 0.8 m), (0.75 m, 0.8 m) and (1.5 m, 1.42 m) respectively. Figure 10 depicts the imaging results given by the traditional TRM method. It is observed that only the first target (the nearest one) can be detected (still with interference). The actual locations of the other two targets can be hardly identified from the resulted images.

On the contrary, successful imaging for all the three targets are achieved based on the proposed method, as shown in Figs. 11 (a), (b), (c) and (d). The results indicate that the proposed TR imaging approach is also applicable for the case where there are more than two targets.

The corresponding optimal time frames obtained by the TIRM algorithm for all the three cases are shown in Table 1.

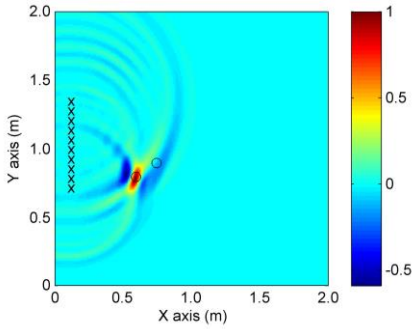

(a)

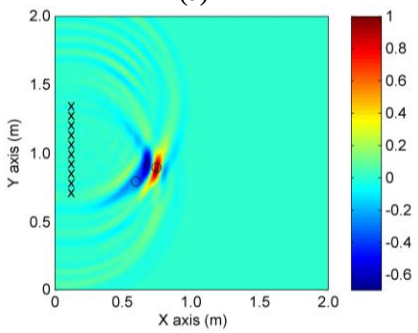

(b)

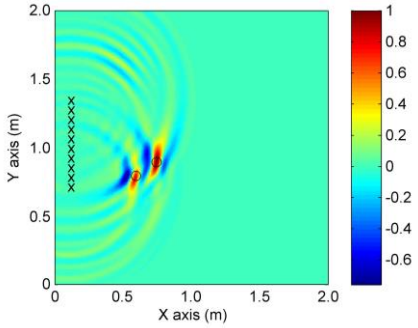

(c)

Fig. 9. Imaging results for the targets located at: (a) (0.6 m, 0.8 m), (b) (0.75 m, 0.9 m), and (c) multiple targets by the proposed TR method.

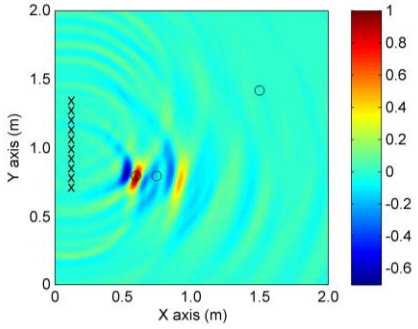

(a)

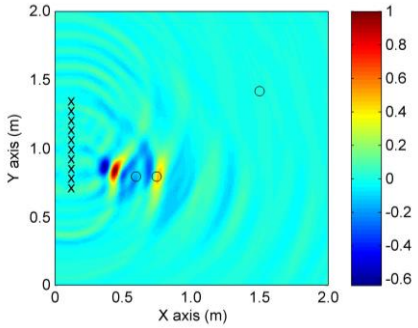

(b)

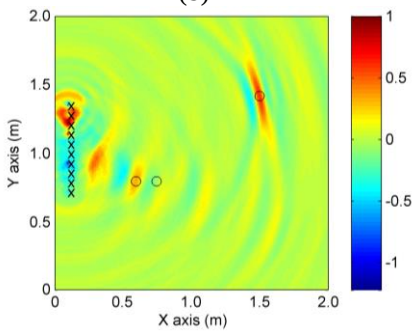

(c)

Fig. 10. Imaging results for the targets located at: (a) (0.6 m, 0.8 m), (b) (0.75 m, 0.8 m), and (c) (1.5 m, 1.42 m) by the traditional TRM method.

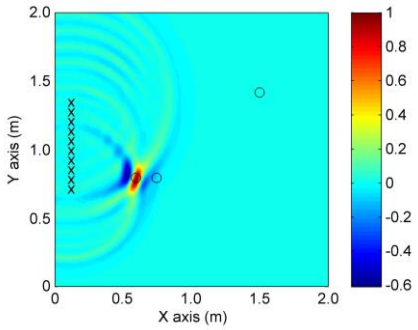

(a)

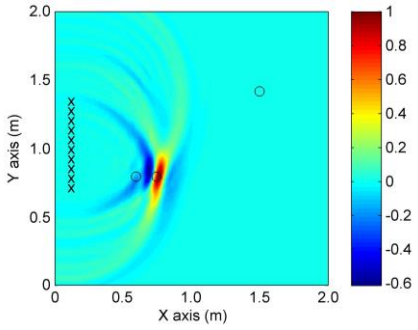

(b)

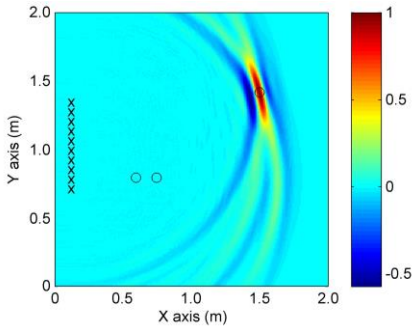

(c)

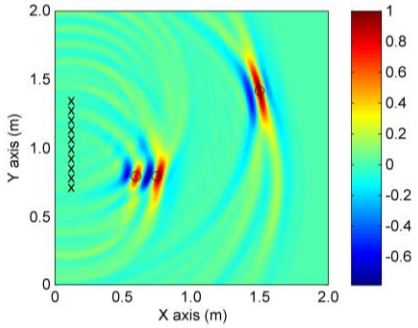

(d)

Fig. 11. Imaging results for the targets located at: (a) (0.6 m, 0.8 m), (b) (0.75 m, 0.9 m), (c) (1.5 m, 1.42 m), and (d) multiple targets by the proposed TR method.

Table 1: Optimal time frames obtained by the TIRM algorithm

Case	Optimal Time Frame/ Δt		
	Target 1	Target 2	Target 3
1	855	698	/
2	855	833	/
3	856	825	670

IV. CONCLUSION

A new TR imaging scheme for multiple targets detection is proposed in this paper. Direct retransmission of the TR signals causes inevitable interferences which are adverse to the identification for the actual targets. To achieve better imaging performance the time domain gating is utilized for the partition of the echo signals. Once the optimal time frame for each target is obtained, all groups of the target responses are time reversed and retransmitted from the TRA. Then the zero setting process is applied to the recorded fields, and imaging for individual target as well as simultaneous multi-targets imaging are carried out based on the new imaging function. Numerical simulation results for three multi-targets cases indicate that satisfactory imaging for the targets can be achieved by the proposed approach which prevails over the traditional TRM method in solving the near-far problem and suppressing the interference fields. Furthermore, it turned out that the proposed scheme is efficient and simple for implementation as it requires only one transmitter and single measurement by the antenna array.

ACKNOWLEDGMENT

This work was supported by the National Natural Science Foundation of China under Grant 61271331 and Grant 61571229.

REFERENCES

[1] M. Fink, D. Cassereau, A. Derode, *et al*., "Time-reversed acoustics," *Reports on progress in Physics*, vol. 63, no. 12, pp. 1933-1995, 2000.

[2] G. Lerosey, J. De Rosny, A. Tourin, *et al*., "Time reversal of electromagnetic waves," *Physical review letters*, vol. 92, no. 19, pp. 193904, 2004.

[3] P. Kosmas and C. M. Rappaport, "Time reversal with the FDTD method for microwave breast cancer detection," *IEEE Trans. Microw. Theory Tech.*, vol. 53, no. 7, pp. 2317-2323, 2005.

[4] S. Sadeghi and R. Faraji-Dana, "A Practical UWB Microwave Imaging System Using Time-Domain DORT for Tumor Detection," *Applied Computational Electromagnetics Society Journal*, vol. 31, no. 6, pp. 692-699, 2016.

[5] R. C. Qiu, C. Zhou, N. Guo, *et al*., "Time reversal with MISO for ultrawideband communications: Experimental results," *IEEE Antennas and Wireless Propagation Letters*, vol. 5, no. 1, pp. 269-273, 2006.

[6] H. T. Nguyen, I. Z. Kovcs and P. C. F. Eggers, "A time reversal transmission approach for multiuser UWB communications," *IEEE Trans. Antennas Propag.*, vol. 54, no. 11, pp. 3216-3224, 2006.

[7] T. Leutenegger and J. Dual, "Non-destructive testing of tubes using a time reverse numerical simulation (TRNS) method," *Ultrasonics*, vol. 41, no. 10, pp. 811-822, 2004.

[8] C. Fan, M. Pan, F. Luo, *et al*., "Multi-frequency time-reversal-based imaging for ultrasonic non-destructive evaluation using full matrix capture," *IEEE Trans. Ultrason., Ferroelectr., Freq. Control*, vol. 61, no. 12, pp. 2067-2074, 2014.

[9] X. Zhu, Z. Zhao, W. Yang, *et al*., "Iterative time-reversal mirror method for imaging the buried object beneath rough ground surface," *Progress In Electromagnetics Research*, vol. 117, pp. 19-33, 2011.

[10] Y. Li and M. Xia, "Time Reversal Imaging Based on Synchronism," *IEEE Antennas and Wireless Propagation Letters*, vol. 16, pp. 2058-2061, 2017.

[11] M. E. Yavuz and F. L. Teixeira, "Full time-domain DORT for ultrawideband electromagnetic fields in dispersive, random inhomogeneous media," *IEEE Trans. Antennas Propag.*, vol. 54, no. 8, pp. 2305-

2315, 2006.

[12] T. Zhang, P. C. Chaumet, A. Sentenac, *et al*., "Improving three-dimensional target reconstruction in the multiple scattering regime using the decomposition of the time-reversal operator," *Journal of Applied Physics*, vol. 120, no. 24, pp. 243101, 2016.

[13] E. A. Marengo and F. K. Gruber, "Subspace-based localization and inverse scattering of multiply scattering point targets," *EURASIP Journal on Advances in Signal Processing*, vol. 2007, no. 1, pp. 017342, 2006.

[14] R. Solimene and A. Dell'Aversano, "Some remarks on time-reversal MUSIC for two-dimensional thin PEC scatterers," *IEEE Geoscience and Remote Sensing Letters*, vol. 11, no. 6, pp. 1163-1167, 2014.

[15] H. Choi, Y. Ogawa, T. Nishimura, *et al*., "Iterative angle-and-time-domain gating technique for time-reversal MUSIC imaging," *Signal processing*, vol. 111, pp. 39-49, 2015.

[16] A. B. Gorji and B. Zakeri, "Time-reversal through-wall microwave imaging in rich scattering environment based on target initial reflection method," *Applied Computational Electromagnetics Society Journal*, vol. 30, no. 6, pp. 626-637, 2015.

[17] K. Yee, "Numerical solution of initial boundary value problems involving Maxwell's equations in isotropic media," *IEEE Trans. Antennas Propag.*, vol. 14, pp. 302-307, 1966.

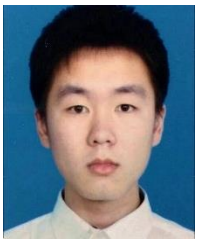

Tong Mu received the B.Eng. degree in Electronic Information Engineering from the Nanjing University of Science and Technology, Nanjing, China, in 2014, where he is currently pursuing the Ph.D. degree in Information and Communication Engineering. His current research interests include microwave imaging and radar signal processing.

Yaoliang Song received the B.Eng., the M.Eng. and the D.Eng. degrees in Electrical Engineering from the Nanjing University of Science and Technology, Nanjing, China, in 1983, 1986 and 2000 respectively. He has been a Researcher Fellow at the Department of Engineering Science at the University of Oxford from Sept. 2004 to Sept. 2005. At present, he is a Professor at Nanjing University of Science and Technology. His major research interests include UWB communications, UWB radar imaging and advanced signal processing.